ADVANCED MATERIALS

Water-Rich Biomimetic Composites with Abiotic Self-Organizing Nanofiber Network

Lizhi Xu, Xueli Zhao, Chuanlai Xu, and Nicholas A. Kotov*

Load-bearing soft tissues, e.g., cartilage, ligaments, and blood vessels, are made predominantly from water (65–90%) which is essential for nutrient transport to cells. Yet, they display amazing stiffness, toughness, strength, and deformability attributed to the reconfigurable 3D network from stiff collagen nanofibers and flexible proteoglycans. Existing hydrogels and composites partially achieve some of the mechanical properties of natural soft tissues, but at the expense of water content. Concurrently, water-rich biomedical polymers are elastic but weak. Here, biomimetic composites from aramid nanofibers interlaced with poly(vinyl alcohol), with water contents of as high as 70–92%, are reported. With tensile moduli of ≈9.1 MPa, ultimate tensile strains of ≈325%, compressive strengths of ≈26 MPa, and fracture toughness of as high as ≈9200 J m^{-2}, their mechanical properties match or exceed those of prototype tissues, e.g., cartilage. Furthermore, with reconfigurable, noncovalent interactions at nanomaterial interfaces, the composite nanofiber network can adapt itself under stress, enabling abiotic soft tissue with multiscale self-organization for effective load bearing and energy dissipation.

Soft tissues, such as articular cartilage, ligaments, tendons, blood vessels, and skin, among others, are based on networks of nanoscale collagen fibers providing high tensile stiffness.[1–4] Noncovalent interactions between collagen, proteoglycan, water, and other biomacromolecules incorporated into these tissues afford high compression stiffness, toughness, and strain,[1,5–8] allowing for reorganization of the nanofibrous network under stress that adapt to body-specific load patterns. Extensive research efforts have been invested into emulating the mechanics of these essential biomaterials with synthetic approaches. It was found that biomimetic hydrogels with two or more polymer networks provide high fracture toughness.[9–11]

Reinforcement with clay nanosheets,[12] biominerals,[13] cellulose,[14,15] or polymeric fibers[16] enhances tensile stiffness of the hydrogels. Noncovalent interactions, i.e., ionic,[17–19] hydrophobic interactions,[20] and hydrogen bonding,[20,21] increase the compression stiffness or viscoelasticity of the materials. Nevertheless, imparting multiple and mutually contradictory properties, as exemplified by high stiffness, toughness, and water content, results in materials that compromise one essential property at the expense of another. Replicating the combination of physical metrics of natural soft tissues remains challenging. For instance, hydrogels with covalently crosslinked nanoreinforcement have a high tensile modulus of ≈2 MPa at low strains,[12] but they experience fracture or catastrophic softening under tensile strains above a few percent due to the limited deformability of the nanofillers. Hydrogels with multiple polymer networks can be stretched by ≈17 times even with a notch in the sample,[10] but the softness of the constituent polymers result in a tensile modulus of only ≈30 kPa, which is two to four orders of magnitude lower than those of cartilage, ligaments, or tendons. Increasing the stiffness of these hydrogels would otherwise be associated with the sacrifice of water content that is essential for cellular viability in biomedical applications.[11,13] Dense nacre-like composites based on stiff inorganic and soft organic components can exhibit high stiffness and toughness,[22,23] but similar mechanics are difficult to achieve in water-rich (e.g., >70 wt%) embodiments due to the chemical and physical limitations of the mineral constituents. Replicating the physical behaviors of load-bearing soft tissues would require a new class of stiff nanoscale components that are capable of forming porous and reconfigurable networks.

We recently reported that para-aramid, commonly known as Kevlar, can form a nanofibrous dispersion in dimethyl sulfoxide (DMSO).[24] Solution-processable nanoscale versions of Kevlar, i.e., aramid nanofibers (ANFs), retain the high mechanical properties of their macroscale parent, and these materials have served as the building blocks for high-strength flexible conductors and battery separators.[24,25] In the context of this study, a key fact is that ANFs with diameters of 5–30 nm and lengths of 3–10 µm form networked structures when DMSO is exchanged with water.[25] Their structural similarity to biological nanofibers, such as those from collagen and those that display extensive branching,[26] inspired us to explore ANFs as the stiff

Dr. L. Xu, Prof. N. A. Kotov
Department of Chemical Engineering and Department
of Materials Science and Engineering
University of Michigan
Ann Arbor, MI 48109, USA
E-mail: kotov@umich.edu
X. Zhao, Prof. C. Xu
State Key Lab of Food Science and Technology
International Joint Research Laboratory for Biointerface
and Biodetection, and School of Food Science and Technology
Jiangnan University
Wuxi, Jiangsu 214122, P. R. China

The ORCID identification number(s) for the author(s) of this article
can be found under https://doi.org/10.1002/adma.201703343.

**ADVANCED
SCIENCE NEWS**

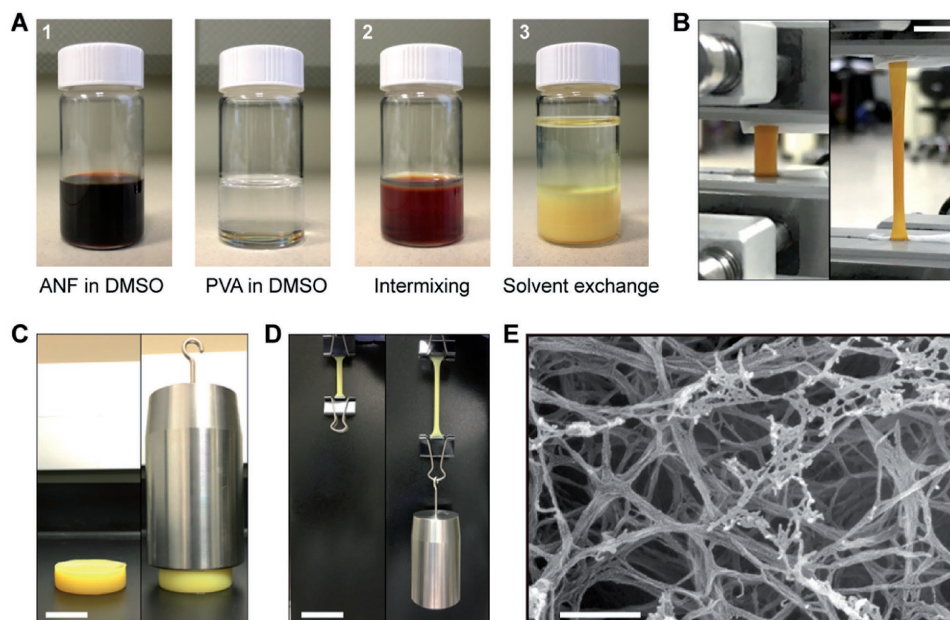www.advancedsciencenews.com

**ADVANCED
MATERIALS**

www.advmat.de

Figure 1. Stiff, tough, and stretchable hydrogels from nanofibrous ANF–PVA composites. A) Photographs of the material components illustrating the facile processing steps for ANF–PVA composite hydrogels. B) A sample of ANF–PVA 30 hydrogel with 0% (left) and 300% (right) tensile strains. Scale bar: 10 mm. C) A sample of ANF–PVA 8 hydrogel with (right) and without (left) a compressive load of 10 N. Scale bar: 30 mm. D) A sample of ANF–PVA 8 hydrogel with (right) and without (left) a tensile load of 10 N. Scale bar: 50 mm. E) An SEM image of a ANF–PVA 8 sample prepared with supercritical CO_2 drying. Scale bar: 300 nm.

components of biomimetic composites.[27] Simultaneously, they offer the possibility of noncovalent interactions with soft polymers. The adaptive interplay between stiff and soft components may lead to synergistic stiffening and toughening.

Preparation of the composite hydrogels starts by separately dissolving poly(vinyl alcohol) (PVA) and para-aramid (poly(p-phenylene terephthalamide), or PPTA) fibers in DMSO (**Figure 1**A). PVA is a biocompatible polymer that has been used in a variety of hydrogels.[28,29] The hydroxyl groups on the PVA chains permit their solubility in DMSO and facilitate intermolecular interactions with ANFs via hydrogen bonding. Mixing ANF dispersion and a PVA solution leads to a viscous fluid that can be molded into various shapes (Figure S1, Supporting Information). A hydrogel with the distinct color of aramid forms when the DMSO is replaced by water (Figure 1A). The hydrogels primarily used in this study have an ANF-to-PVA ratio of 1:5 with two different water content levels, denoted as ANF–PVA 8 (≈92 wt% water) and ANF–PVA 30 (≈70 wt% water). These ANF–PVA hydrogels exhibit unusually high stiffness, toughness, and stretchability (Figure 1B–D). Scanning electron microscopy (SEM) reveals the microscale morphology of the ANF–PVA hydrogels, wherein nanofibers form uniform and highly interconnected networks (Figure 1E) facilitated by flexibility and branching of the individual ANFs.[26] The structures of ANF–PVA and neat ANF hydrogels are similar (Figure S3, Supporting Information), indicating the role of ANFs as the framework of the composites. The characteristic geometrical parameters of ANF–PVA network are nearly identical to those in collagen-based soft tissues (Figure S2, Supporting Information). The mechanical properties of ANF–PVA hydrogels were characterized by tensile and compression tests (**Figure 2**). Hydrogels made from ≈2 wt% ANF and ≈98 wt%

water without PVA, denoted as ANF 2, were also analyzed for comparison. ANF–PVA 30 has a tensile modulus of as high as ≈9.1 MPa (Figure 2A). The tensile modulus of ANF–PVA 8 (≈1.9 MPa) is slightly lower than that of ANF 2 (≈2.2 MPa), in line with the lower ANF content. These observations indicate that the 3D network of ANF is mainly responsible for the high tensile stiffness of the composite hydrogels. The ultimate tensile strains, however, show drastic differences between ANF–PVA composite hydrogels and ANF 2. While ANF–PVA 30 and ANF–PVA 8 can withstand high tensile strains up to ≈325% and ≈70%, respectively, ANF 2 fractures at a strain of ≈9%. Both ANF–PVA 8 and ANF–PVA 30 show hysteresis under cyclic tensile strains, and retain ≈91% (Figure 2C) and ≈97% (Figure 2E) of the maximum stresses after five cycles of 20% strain, respectively. Strain-rate-dependent moduli attest to the viscoelasticity of the hydrogels (Figure S4, Supporting Information). In addition, Mullins' effect, a typical behavior of soft tissues, can be seen as the dependence of stress–strain curves on the loading history (Figure S5, Supporting Information). This behavior indicates structural reconfigurability of ANF–PVA composites. It is also conducive to high energy dissipation. Indeed, notched samples of ANF–PVA 30 and ANF–PVA 8 reveal unusual fracture energies of as high as ≈9200 J m^{-2} (Figure S6, Supporting Information) and ≈2300 J m^{-2} (Figure S7, Supporting Information), respectively; the former value is comparable to that of natural rubbers and ≈10 times higher than that of articular cartilage.[8,10]

ANF–PVA 8 and ANF–PVA 30 also show high compressive moduli of ≈1.0 MPa and ≈4.0 MPa, respectively. These values exceed those of ANF 2 (≈0.3 MPa) by two and twelve times (Figure 2B), respectively, indicating the essential role of PVA. A small amount of water escapes from the surface of the
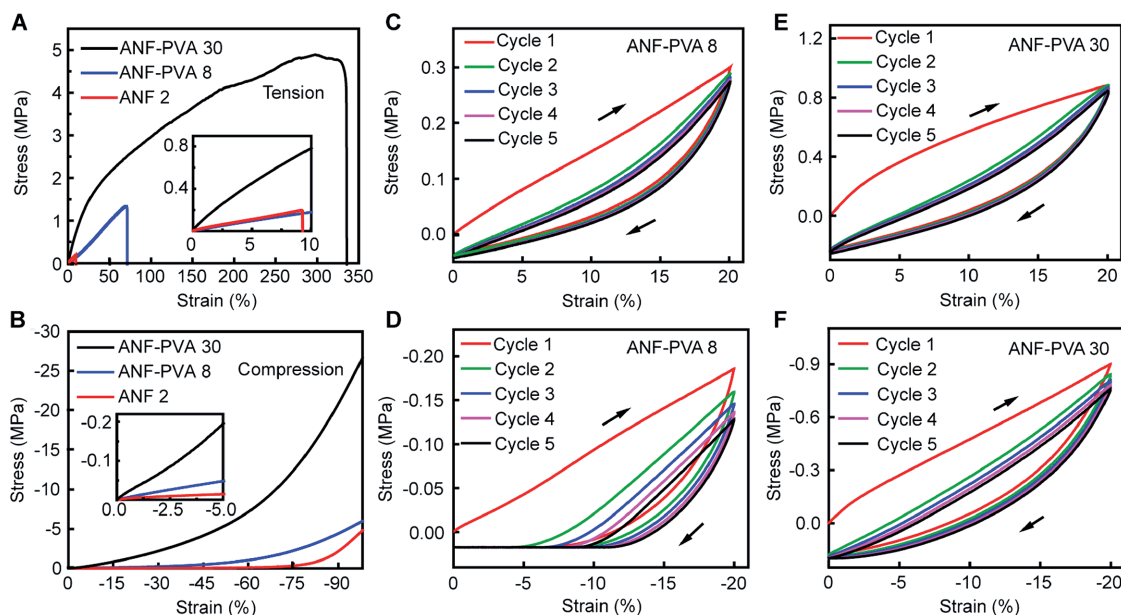
Figure 2. Quantitative mechanical characterization of ANF–PVA composite hydrogels. A,B) Stress–strain curves for ANF 2, ANF–PVA 8, and ANF–PVA 30 obtained from uniaxial tensile (A) and compression (B) tests. Insets show magnified plot with low strains. C–F) Cyclic stress–strain curves for ANF–PVA 8 (C,D) and ANF–PVA 30 (E,F) with five cycles of 20% tensile (C,E) and compressive (D,F) strains, respectively. All the samples were immersed in water for at least 3 d before testing.

hydrogels during the mechanical tests, which resembles the behavior of connective tissues. Notably, their high compressive stiffness originates from impeded flow of interstitial water through the swelled proteoglycan.[1] Similarly to the prototype tissues, PVA in the composite network retains a high volume of interstitial water and restricts its flow through the fibrous mesh, which provides high compression resistance. This point is further supported by the observation that ANF–PVA hydrogels with lower solid content, i.e., ANF–PVA 8, show larger hysteresis than ANF–PVA 30 (Figure 2D,F). This flow-dependent viscoelasticity is known to provide critical friction-reducing and/or energy-dissipating functionalities to load-bearing soft tissues.[1]

Fourier transform infrared (FTIR, **Figure 3**A,B) and Raman scattering spectroscopy (Figure S8, Supporting Information) provide insights into the ANF–PVA interactions. One can identify a distinct red-shift of the aramid C=O stretching band in ANF–PVA composites compared to bare ANF (Figure 3B), evidencing hydrogen bonding between the stiff and soft components (Figure 3C). The essential role of hydrogen bonds in the macroscale mechanics of ANF–PVA hydrogels is confirmed by a drastic reduction of their mechanical strength (Figure S9, Supporting Information) in high-concentration urea solution, which disrupts hydrogen bonds. Concurrently, lowering the molecular weight of the PVA used in ANF–PVA composites from 146 000–186 000 a.u. to 13 000–23 000 a.u. results in a decrease of the mechanical strength of the hydrogels from ≈5.9 MPa to ≈0.2 MPa (Figure S10, Supporting Information).

Extensive interfacial interactions between nanoscale components are essential in biological tissues and are responsible for many of their exceptional functionalities.[1,30–32] The method of composite synthesis described here maximizes nanomaterials interaction which leads to the distinct behaviors of ANF–PVA hydrogels. DMSO is a polar aprotic solvent and a strong hydrogen bond acceptor, which inhibits hydrogen bond formation between PVA and ANF. Perhaps counter intuitively, this inhibition is essential for engineering hydrogen bonding for biomimetic nanocomposites. The inhibition of interactions between ANFs and PVA prevent gelation that is unwanted at this stage, allowing for uniform mixing and interfacial contact. Upon solvent exchange with water, a weaker hydrogen bond acceptor, the hydroxyl groups on PVA become available to interact with the carbonyl groups on ANFs. Although a competition for hydrogen bonds does exist in water, extensive hydrogen bonding between ANF and PVA takes place due to the energetically favorable O—H···O=C interaction[33] and the cooperativity of supramolecular interactions involving two macromolecular components.

Cooperative effects stabilize the hydrogen bonding in hydrogels.[21] As an indication of their role in the deformation of ANF–PVA networks, the utilization of PVA with different degrees of hydrolysis (99%+ and 87%, respectively) results in drastic changes in the mechanics of the ANF–PVA hydrogels (Figure S11, Supporting Information). The acetate side groups in less-hydrolyzed PVA hinder the cooperative formation of hydrogen bonds and lead to lower stiffness and strength of the composite hydrogels.

The reconfigurable, noncovalent interactions between ANF and PVA lead to synergistic interplay and self-organization behavior under stress. The hydrogen-bonded PVA chains bridge the fibrous ANF network and facilitate load transfer through the stiff aramid skeleton. Furthermore, hydrogen bonds reforming in response to PVA reconfiguration allow plastic deformation of the fibrous network accompanied by high energy dissipation (Figure 3D). Characteristic fiber alignment can be seen at the tear surfaces of ANF–PVA hydrogels (Figure 3I,J). Similar effect (Figure S12, Supporting Information) also explains the
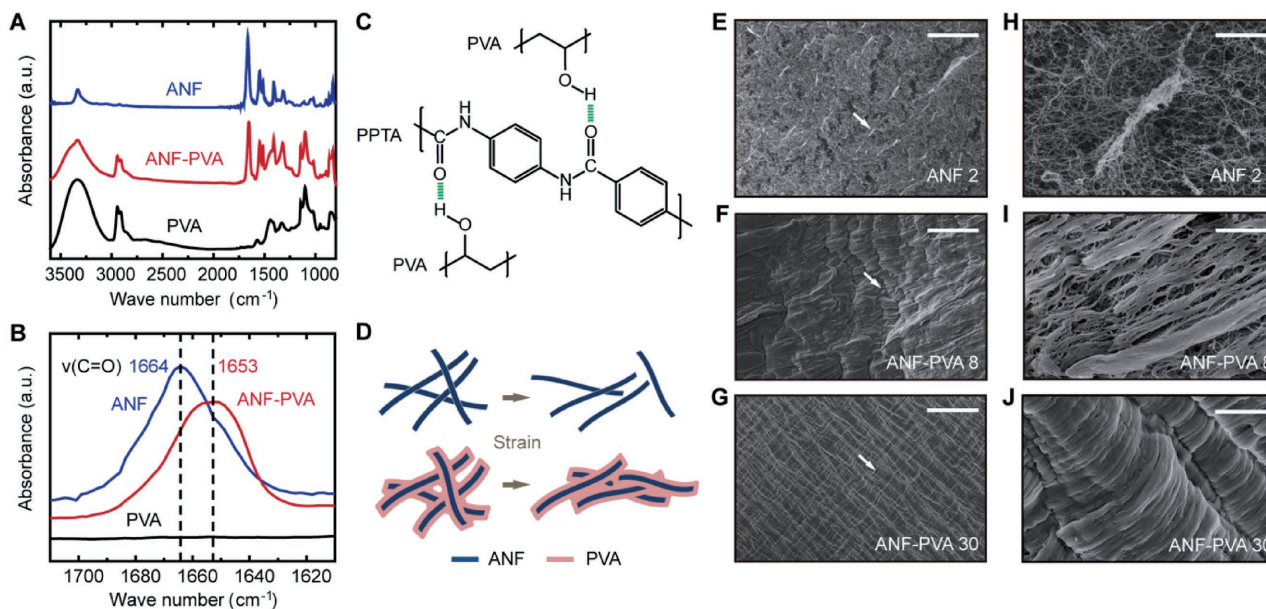
**ADVANCED
SCIENCE NEWS**

www.advancedsciencenews.com

**ADVANCED
MATERIALS**

www.advmat.de

Figure 3. Chemistry and self-organization behaviors of ANF–PVA composite networks. A) FTIR spectra of ANF, PVA, and ANF–PVA composites. B) Magnified plot of FTIR spectra showing the peak positions associated with the aramid C=O stretching vibration. C) Chemical structures of PPTA and PVA, and schematics of their hydrogen bonding interactions. D) Schematics of ANF and ANF–PVA composites and their different strain behaviors. The ANF–PVA network self-organizes in response to strain, while bare ANF networks experience fracture. E–G) SEM images of fracture surfaces of ANF 2 (E), ANF–PVA 8 (F), and ANF–PVA 30 (G), prepared from tearing tests on notched samples. Scale bars: 30 μm. H–J) Magnified SEM images of fracture surfaces of ANF 2 (H), ANF–PVA 8 (I), and ANF–PVA 30 (J). Scale bars: 2 μm.

strain-stiffening behavior after multiple loading-unloading cycles (Figure 2C,E). One can also notice that the greater volumetric density of the intermolecular interactions in ANF–PVA 30 results in a higher degree of organization (Figure 3J) than that in ANF–PVA 8 (Figure 3I). Naturally, ANF 2 experiences brittle fracturing with minimal reorganization of the network (Figure 3H) at molecular, nano, and micrometer scales. Therefore, the differences in toughness and ultimate tensile strains between ANF–PVA 30, ANF–PVA 8 and ANF 2 can be attributed to their different abilities to reorganize under stress.

Similar processes of fiber realignment, stress adaptation, and nearly identical microscale patterns are observed in tendons, ligaments and artery walls based on collagen-proteoglycan networks.[31] We note that the ANF–PVA 30 composite exhibits a greater degree

of reorganization under fracture than that of cartilage,[34] which is consistent with its higher fracture toughness. Therefore, ANF–PVA can serve as an abiotic materials platform replicating load-bearing soft-tissues based on the reconfigurable 3D nanofibrous network. Self-healing behaviors associated with the reconfigurable nanomaterials interactions could also be further explored.

In contrast to many hydrogels which experience dramatic swelling and weakening in aqueous environment, ANF–PVA hydrogels exhibit little changes in volume or mechanical characteristics when chronically immersed in phosphate buffered saline at 37 °C (Figure S13 and S14, Supporting Information), indicating their potential utilities in physiological conditions. The cumulative metrics of ANF–PVA (**Table 1**; Table S1, Supporting Information) and their biocompatibility (Figure S15,

Table 1. Quantitative comparison of the physical properties of ANF–PVA composite hydrogels with other strong synthetic hydrogels and articular cartilage. The ANF–PVA hydrogels possess a rare combination of mechanical properties where each individual parameter is similar to or exceeds those of some of the current best-in-class synthetic hydrogels. Their mechanical behaviors are parallel to those of articular cartilage, while the fracture energy of ANF–PVA 30 can even be ≈10 times higher than that of the natural counterpart.

Hydrogel type	Reference	Water content [wt%]	Tensile modulus [MPa]	Tensile strength [MPa]	Compressive modulus [MPa]	Compressive strength [MPa]	Fracture energy [J m^{-2}]
ANF–PVA	Present work	92–70	1.9–9.1	1.4–5.0	1.0–4.0	5.9–26.5	2300–9200
Multiple network	[9–11]	90–65	0.03–1.4	0.2–1.4		≈17	100–14 000
Clay composites	[12]	70	≈2[a]	≈3[a]			
Cellulose composites	[14,15]	90–68	1–23[a]	1–3.8[a]	1.3–3.9[a]	2.1–5.3[a]	
PVA cryogels	[28,29]	90–75	≈0.2	≈0.6	≈0.8	≈1.7	
Ionic crosslinking	[18,19]	70–50	0.5–2	2–6			≈4000
Articular cartilage	[3–8]	80–65	1–10	1–20	0.5–10	10–50	500–1500

[a]Anisotropic (highest values are shown).

Supporting Information) reveal their promise for engineering of soft tissues.[35]

ANF–PVA composites can also be compared to another class of biomaterials made from stiff and soft components known as nacre- or bone-mimics. The noncovalent interactions between stiff ANF and soft PVA are, in fact, similar to the reconfigurable lustrin A-aragonite ionic bonds in nacres.[32] These bonds are critical for combining high stiffness and toughness.[30,32] One of the challenges of artificial nacre is to increase its ductility,[22,23,36] which is difficult due to the ionic nature of the chemical bonds in the stiff inorganic phase of biomineralized tissues, as well as their high volumetric threshold for percolation. The utilization of ANFs as the stiff components facilitates 3D network formation and eliminates the orthogonality of the chemistries between the soft and hard components, which leads to better integration and more efficient load transfer at their interface. These effects are essential for replication of stiff and tough biological materials with high water content capable of supporting living tissues.

In conclusion, the ANF–PVA composites made from stiff aramid fibrils bridged by soft PVA matrices are able to reconcile exceptional mechanics with the requisite high water content in soft tissues. They replicate the key structural patterns of collagen–proteoglycan networks at molecular, nanoscale, and mesoscale levels. The abilities of ANFs to carry high loads and to form reconfigurable networks with water-retaining polymer components form the foundation for development of a wide spectrum of load-bearing biomaterials. The properties are also essential for a variety of applications requiring durability and high mass transport. Biomimetic ANF–PVA composites can also serve as high-transport nanoporous membranes in fuel cells, water desalination units, batteries, and filters.

Experimental Section

Preparation of ANF–PVA Hydrogels: A 2 wt% ANF dispersion in DMSO was prepared using methods described elsewhere,[25] and mixed with an equal volume of a 10 wt% PVA (Sigma–Aldrich, M_w 146 000–186 000 a.u., 99%+ hydrolyzed) solution in DMSO. The mixing ratio was optimized for both the stiffness and strength of the resulting hydrogels (Figure S16, Supporting Information). Excess DMSO in the mixture can be evaporated in a vacuum oven for further control of the solid content. The mixture was then casted in custom-designed molds and submerged in deionized water for 24 h to generate ANF–PVA hydrogels with desired 3D geometries. Supercritical CO_2 drying (Leica CPD 300) was applied to the samples for SEM imaging, FTIR, or Raman scattering spectroscopy. The weight fraction of water/solid content was determined by comparing the wet weight of the hydrogels to their dry weights after baking in a 100 °C vacuum oven for 24 h.

We note that the preparatory steps involving mixing in DMSO and subsequent solvent exchange are crucial for acquiring the molecular scale integration of ANF and PVA and the high density of hydrogen bonding in these nanocomposite hydrogels. Other techniques, for instance the direct infiltration of ANF 3D networks with another polymer, do not result in similar mechanical properties because the diffusion of high-molecular-weight PVA into the nanofiber network is impeded not only by the small pore size but also the hydrogen-bonded, immobilized PVA chains at the interfaces. For instance, premade ANF networks infiltrated with aqueous PVA solution exhibit only ≈50% of the mechanical strength of their counterparts prepared via mixing in DMSO (Figure S17, Supporting Information).

Mechanical Testing: A mechanical testing machine (TA.XT *plus*, Texture Technologies) was used for both tensile and unconfined compressive tests with a standard strain rate of 0.2% per second. Engineering stress (σ)–strain (ε) curves were analyzed with effective tensile/compressive moduli defined as $E = \sigma/\varepsilon$ at $\varepsilon = \pm5\%$, respectively. Fracture energy was determined following an established method,[10] whereby tensile tests are applied on notched samples and compared with the results of unnotched samples for fracture energy calculations (Figure S6 and S7, Supporting Information).

Evaluation of Biocompatibility: Human cartilage cells were cultured on ANF–PVA 8 composite hydrogels (experimental group) or in wells without hydrogels (control group) in glass-bottomed Petri dishes (Nest Biotechnology Co., Ltd.). A LIVE/DEAD cell imaging kit 488/570 (ThermoFisher Scientific) was used for confocal fluorescence microscope imaging (Leica TCS SP8) with excitation wavelengths of 488 and 552 nm. Live cells were stained with cell-permeable dye, and dead cells were stained with cell-impermeable dye.

Supporting Information

Supporting Information is available from the Wiley Online Library or from the author.

Conflict of Interest

N.A.K. is a co-founder of a company Elegus Technologies commercializing ANF materials.

[1] X. L. Lu, V. C. Mow, *Med. Sci. Sports Exercise* **2008**, *40*, 193.

[2] A. Sharma, A. J. Licup, K. A. Jansen, R. Rens, M. Sheinman, G. H. Koenderink, *Nat. Phys.* **2016**, *12*, 584.

[3] S. L. Woo, W. H. Akeson, G. F. Jemmott, *J. Biomech.* **1976**, *9*, 785.

[4] A. K. Williamson, A. C. Chen, K. Masuda, E. J. M. A. Thonar, R. L. Sah, *J. Orthop. Res.* **2003**, *21*, 872.

[5] C. G. Armstrong, V. C. Mow, *J. Bone Jt. Surg.* **1982**, *64*, 88.

[6] E. M. H. Obeid, M. A. Adams, J. H. Newman, *J. Bone Jt. Surg.* **1994**, *76-B*, 315.

[7] A. J. Kerin, M. R. Wisnom, M. A. Adams, *Proc.- Inst. Mech. Eng.* **1998**, *212*, 273.

[8] N. K. Simha, C. S. Carlson, J. L. Lewis, *J. Mater. Sci.: Mater. Med.* **2003**, *14*, 631.

[9] J. P. Gong, Y. Katsuyama, T. Kurokawa, Y. Osada, *Adv. Mater.* **2003**, *15*, 1155.

[10] J.-Y. Sun, X. Zhao, W. R. K. Illeperuma, O. Chaudhuri, K. H. Oh, D. J. Mooney, J. J. Vlassak, Z. Suo, *Nature* **2012**, *489*, 133.

[11] J. Li, Z. Suo, J. J. Vlassak, *J. Mater. Chem. B* **2014**, *2*, 6708.

[12] J. Wang, L. Lin, Q. Cheng, L. Jiang, *Angew. Chem., Int. Ed.* **2012**, *51*, 4676.

[13] N. Rauner, M. Meuris, M. Zoric, J. C. Tiller, *Nature* **2017**, *543*, 407.

[14] A. Nakayama, A. Kakugo, J. P. Gong, Y. Osada, M. Takai, T. Erata, S. Kawano, *Adv. Funct. Mater.* **2004**, *14*, 1124.

[15] S. Liang, J. Wu, H. Tian, L. Zhang, J. Xu, *ChemSusChem* **2008**, *1*, 558.

[16] F. T. Moutos, L. E. Freed, F. Guilak, *Nat. Mater.* **2007**, *6*, 162.

[17] M. Liu, Y. Ishida, Y. Ebina, T. Sasaki, T. Hikima, M. Takata, T. Aida, *Nature* **2014**, *517*, 68.

[18] T. L. Sun, T. Kurokawa, S. Kuroda, A. Bin Ihsan, T. Akasaki, K. Sato, T. Nakajima, J. P. Gong, M. A. Haque, T. Nakajima, J. P. Gong, M. A. Haque, *Nat. Mater.* **2013**, *12*, 932.

[19] P. Lin, S. Ma, X. Wang, F. Zhou, *Adv. Mater.* **2015**, *27*, 2054.

[20] M. Guo, L. M. Pitet, H. M. Wyss, M. Vos, P. Y. W. Dankers, E. W. Meijer, *J. Am. Chem. Soc.* **2014**, *136*, 6969.

[21] G. Song, L. Zhang, C. He, D. C. Fang, P. G. Whitten, H. Wang, *Macromolecules* **2013**, *46*, 7423.

[22] Z. Tang, N. A. Kotov, S. Magonov, B. Ozturk, *Nat. Mater.* **2003**, *2*, 413.

[23] L.-B. Mao, H.-L. Gao, H.-B. Yao, L. Liu, H. Cölfen, G. Liu, S.-M. Chen, S.-K. Li, Y.-X. Yan, Y.-Y. Liu, S.-H. Yu, *Science* **2016**, *354*, 107.

[24] S.-O. Tung, S. Ho, M. Yang, R. Zhang, N. A. Kotov, *Nat. Commun.* **2015**, *6*, 6152.

[25] J. Lyu, X. Wang, L. Liu, Y. Kim, E. K. Tanyi, H. Chi, W. Feng, L. Xu, T. Li, M. A. Noginov, C. Uher, M. D. Hammig, N. A. Kotov, *Adv. Funct. Mater.* **2016**, *26*, 8435.

[26] J. Zhu, M. Yang, A. Emre, J. H. Bahng, L. Xu, J. Yeom, B. Yeom, Y. Kim, K. Johnson, P. Green, N. A. Kotov, *Angew. Chem., Int. Ed.* **2017**, *56*, 11744.

[27] P. Podsiadlo, A. K. Kaushik, B. S. Shim, A. Agarwal, Z. Tang, A. M. Waas, E. M. Arruda, N. A. Kotov, *J. Phys. Chem.* **2008**, *112*, 14359.

[28] Y. Mori, H. Tokura, M. Yoshikawa, *J. Mater. Sci.* **1997**, *32*, 491.

[29] J. A. Stammen, S. Williams, D. N. Ku, R. E. Guldberg, *Biomaterials* **2001**, *22*, 799.

[30] U. G. K. Wegst, H. Bai, E. Saiz, A. P. Tomsia, R. O. Ritchie, *Nat. Mater.* **2014**, *14*, 23.

[31] R. H. Pritchard, Y. Y. S. Huang, E. M. Terentjev, *Soft Matter* **2014**, *10*, 1864.

[32] B. L. Smith, T. E. Schaffer, M. Viani, J. B. Thompson, N. A. Frederick, J. Kindt, A. Belcher, G. D. Stucky, D. E. Morse, P. K. Hansma, *Nature* **1999**, *399*, 761.

[33] T. Steiner, *Angew. Chem., Int. Ed.* **2002**, *41*, 49.

[34] I. C. Clarke, *J. Bone Jt. Surg.* **1971**, *53-B*, 732.

[35] E. S. Place, J. H. George, C. K. Williams, M. M. Stevens, *Chem. Soc. Rev.* **2009**, *38*, 1139.

[36] Y. Lu, Y. Yang, A. Sellinger, M. Lu, J. Huang, H. Fan, R. Haddad, G. Lopez, A. R. Burns, D. Y. Sasaki, J. Shelnutt, C. J. Brinker, *Nature* **2001**, *410*, 913.